High Power Laser Science and Engineering, (2024), Vol. 12, e82, 8 pages.
doi:10.1017/hpl.2024.68

HIGH POWER LASER SCIENCE AND ENGINEERING

RESEARCH ARTICLE

High-power, ultra-low-noise cascaded diamond Raman lasers with spectrum compression

Hui Chen[1,2], Zhongan Zhao[1,2], Wenqiang Fan[1,2], Yunpeng Cai[1,2], Boyuan Zhang[1,2], Jie Ding[1,2], Yaoyao Qi[1,2], Bingzheng Yan[1,2], Yulei Wang[1,2], Zhiwei Lu[1,2], and Zhenxu Bai[1,2]

[1] *Center for Advanced Laser Technology, Hebei University of Technology, Tianjin, China*

[2] *Hebei Key Laboratory of Advanced Laser Technology and Equipment, Tianjin, China*

(Received 11 July 2024; revised 10 September 2024; accepted 29 September 2024)

Abstract

Stimulated Raman scattering is a third-order nonlinear optical effect that is not only effective for wavelength converting laser output, but also for single longitudinal-mode output due to the absence of spatial hole burning. Diamond is a prominent Raman-active medium that has significant potential for linewidth narrowing and wavelength converting lasers at high power levels due to its high thermal conductivity, long Raman frequency shift and wide spectral transmission range. In this work we utilize diamond in a resonantly mode-matched external cavity to achieve cascaded Raman conversion of a 1064 nm laser. By fine-tuning the length of this external cavity, we can obtain narrow linewidth emission at 1240 and 1485 nm. When operating at maximum power, the measured linewidths were more than twofold narrower than the linewidth of the fundamental field. In addition, the noise levels of the Stokes fields are lower than that of the fundamental field throughout the entire noise frequency range, and the intrinsic linewidth of the second Stokes field, which is expressed at the hertz level (~3.6 Hz), is decreased by approximately three orders of magnitude compared to that of the pump. This work represents the first measurement and analysis of the linewidth and noise characteristics of cascaded diamond Raman lasers and, significantly, offers a new means by which high-power, narrow linewidth laser output can be produced from wavelength-converted laser systems.

Keywords: cascade; diamond Raman laser; high power; low noise; narrow linewidth

1. Introduction

Narrow linewidth lasers are essential tools used across a plethora of high-precision measurement and scientific applications, including gravitational wave detection[1], quantum optics[2], laser guide stars[3] and laser cooling[4]. In addition to a narrow linewidth, these applications can also have other significant laser requirements pertaining to wavelength and output power. The wavelength output range of conventional particle inversion lasers can be limited, owing to the characteristics of the atomic transition energy levels of their gain medium. Furthermore, the linewidth of these lasers can also be affected by spatial hole burning (SHB) (a periodic modulation of the gain within the laser gain medium[5]), which usually results in an output with multiple longitudinal modes (and hence broad linewidth). The impact of SHB can be alleviated using unidirectional annular cavities[6], short cavity methods[7], frequency-selective elements[8] and seed injection[9]; however, these approaches typically increase system complexity and can limit output power.

Third-order nonlinear frequency conversion processes such as stimulated Raman scattering (SRS) and stimulated Brillouin scattering (SBS) do not involve the storage of energy within the conversion medium, and therefore do not suffer from SHB. Therefore, lasers that utilize these effects can directly generate single longitudinal-mode (SLM) laser output[10–15]. In addition, SRS and SBS are not constrained by phase matching and hence, in theory, laser output at any wavelength within the SRS/SBS-active medium's transparency range can be achieved. The magnitude of the frequency shift achieved using the SRS process is typically two to three orders of magnitude greater than that achieved using SBS. As such, the design characteristics of Raman lasers are typically less constrained/complex than Brillouin lasers, especially in relation to fine control of cascading Stokes orders. In this respect, Raman lasers have greater potential to expand the wavelength range of single-frequency lasers.

Correspondence to: Z. Bai, Center for Advanced Laser Technology, Hebei University of Technology, Tianjin 300401, China. Email: baizhenxu@hotmail.com

In the context of single-frequency lasers, diamond has significant potential to simultaneously enhance the output power and wavelength coverage of such lasers, owing to the ultra-high thermal conductivity of the crystals (>2000 W/mK), extremely broad spectral transmission range (for wavelengths >0.23 μm)[16–20] and outstanding nonlinear optical characteristics. Within the literature, a continuous-wave (CW) SLM 1240 nm Raman laser of output power up to 4 W has been achieved from a free running diamond Raman standing-wave cavity without the need for additional frequency-selective elements[12]. However, it was reported that thermal effects within the cavity led to changes in the cavity length, which limited the system's power scaling capacity. Cavity locking using the Hänsch–Couillaud (HC) technique is an approach that has proven effective at improving the stability and power scalability of SLM diamond Raman lasers, and outputs of up to 7.2 W have been demonstrated[21]. With the adoption of V-shaped cavities, which have lower sensitivity to misalignment and single-mode fluctuation in comparison to linear cavities, CW SLM diamond Raman laser outputs have been scaled to powers of up to 20 W[13,22]. The large Raman shift in diamond in conjunction with cascading of Stokes orders highlights the expansive breadth of wavelengths that can be achieved when using this crystal for SRS. Furthermore, this wavelength diversity can be further expanded with the inclusion of other nonlinear optical processes, such as sum-frequency generation/second harmonic generation, expanding the wavelength range of narrow linewidth diamond Raman lasers across both long- and short-wave spectral regions[23–26].

In this paper, we demonstrate the generation of narrow linewidth Raman laser emission at wavelengths of 1240 nm (first Stokes) and 1485 nm (second Stokes) through cascaded SRS conversion using diamond in a simple linear standing-wave cavity structure, without the need for additional frequency-selective elements. The corresponding maximum output powers are 14 and 8 W, respectively. We actively tuned the cavity length to match the Stokes wavelength in order to achieve narrow linewidth output. By measuring the Raman laser linewidth at different output powers, we found that the self-heterodyne-measured linewidths of the first and second Stokes fields were compressed by more than twofold in comparison to that of the pump/fundamental field. Analysis of the noise characteristics of the laser showed that the second Stokes field had significantly lower noise than the pump/fundamental field. To the best of our knowledge, this work constitutes the first characterization and measurement of the linewidth and noise of a cascaded diamond Raman laser.

2. Experimental setup and results

A schematic showing the layout of the diamond Raman laser is shown in Figure 1. A 1064 nm single-frequency CW semiconductor laser (RIO origin RIO0175-5-07-1) was used to seed an ytterbium-doped fiber amplifier that produced a maximum power of 50 W (this was used as the pump/fundamental field input into the cavity). A half-wave plate (λ/2) and an isolator were used to control the power of the fundamental field input into the cavity. Lenses L1 and L2 were used to collimate and adjust the diameter size of the fundamental field to approximately 2.7 mm, ensuring the appropriate pump focusing size at the cavity waist when combined with lens L3. Another λ/2 was used to adjust the polarization direction of the fundamental field so as to be parallel to the <111> axis of the diamond crystal, achieving maximum Raman gain[27]. The Raman medium used in the experiment was a 2 mm × 2 mm × 7 mm chemical vapor deposition (CVD) single crystal diamond with anti-reflection coatings for 1064 nm (fundamental field), 1240 nm (first Stokes field) and 1485 nm (second Stokes field) applied to the two end faces perpendicular to the direction of laser transmission. The diamond was positioned at the beam waist of the cavity, with its four planes parallel to the optical axis surrounded by a copper heatsink. This setup facilitated heat dissipation through water cooling at 20°C to quickly achieve thermal stability and prevent damage to the diamond's coating due to excessive temperatures[28]. The output coupler (OC) was fixed to a piezoelectric-actuated translation stage (PZT) that enabled fine adjustment of the

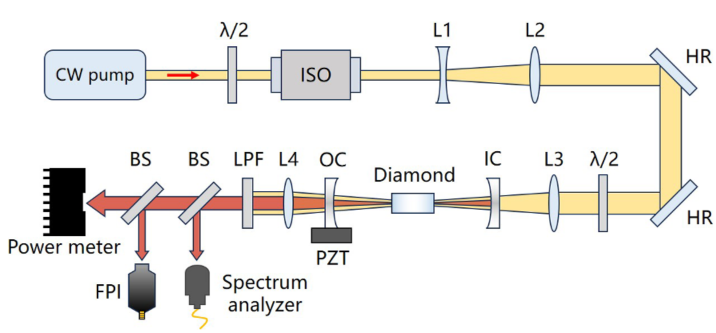

Figure 1. Schematic diagram of the cascaded narrow linewidth diamond Raman laser system. λ/2, half-wave plate; IC, input coupler; OC, output coupler; PZT, piezoelectric-actuated translation stage; LPF, long-pass filter; BS, beam splitter; FPI, Fabry–Pérot interferometer.

https://doi.org/10.1017/hpl.2024.68 Published online by Cambridge University Press

cavity length. In addition, no active cavity locking was implemented in our study; therefore, the resonance of the Raman field was achieved solely through the coating of the cavity mirror. Lens L4 (which had a focal length of 150 mm) and a long-pass filter (LPF) were positioned after the cavity to collimate the output Stokes fields and filter out the residual fundamental field passing through the cavity. In optimizing the output characteristics of the first and second Stokes fields, different cavity parameters (such as output transmittance and cavity length) were used, and these are described in detail in the corresponding sections below.

2.1. Generation of first Stokes emission

To generate the first Stokes emission from the system, a focusing lens L3 with a focal length of 75 mm was used. The input coupler (IC) had a radius of curvature (ROC) of 50 mm and was coated with a high-transmission coating for 1064 nm and a high-reflection coating for 1240 nm. The OC had an ROC of 50 mm and was coated with a high-reflection coating for 1064 nm and a partially transmitting coating ($T = 0.73\%$) for 1240 nm. This configuration enabled double-pass pumping of the diamond crystal. The diamond Raman cavity had a length of approximately 103 mm, with beam waist radii of 30 and 45 μm for the fundamental and first Stokes fields in the diamond, respectively.

Figure 2(a) is a plot showing the power-transfer characteristics of the first Stokes field as a function of the incident fundamental field/pump power, along with the residual fundamental power passing through the cavity. The threshold for first Stokes generation was approximately 13 W, and at a maximum fundamental power of 45.5 W, a first Stokes output power of 14.5 W was achieved, corresponding to a conversion efficiency of 31.8% and a slope efficiency of 44.6%. Shown in the inset is the spatial intensity profile of the first Stokes field at 1240 nm. We used a wavelength meter (HighFinesse WS7-60) to measure the wavelength stability of the first Stokes output over a period of 10 minutes and this is plotted in Figure 2(b). The plot indicates that for a first Stokes output power of 10 W, the center wavelength of the first Stokes field fluctuates within a bandwidth of approximately 68 MHz over a period of around 13 minutes, while the root mean square (RMS) variation of the output power remains around 1% during SLM operation. However, due to temperature fluctuations and environmental vibrations, mode jumping occurred afterward, leading to a transition to multi-longitudinal-mode (MLM) operation.

To investigate the longitudinal-mode characteristics of the generated Stokes fields, we utilized a spectrum analyzer (AQ6370D, Yokogawa) and a scanning Fabry–Pérot interferometer (FPI, SA210-8B, Thorlabs). We observed that as the Stokes output power changed, so did its spectral characteristics, specifically its longitudinal-mode characteristics. These changes were due to differing thermal intensities manifesting within the cavity caused by changes in power. These thermal fluctuations had the net effect of altering the length of the cavity. In order to counter these undesired changes in cavity length, for specific operating points, we actively adjusted the cavity length using a PZT (using adjustment step sizes of approximately 30 nm) while monitoring the output spectrum and FPI transmission signal. Representative plots of the outputs that we recorded are shown in Figure 3; the left-hand panels of plots show the measured first Stokes output spectrum, while the right-hand panels of plots show the corresponding FPI transmission signal. As can be seen from the spectra, the center wavelength is approximately 1240 nm. As the cavity length changes, the morphology of the spectral output switches between smooth and rough states. Specifically, the smooth spectral state corresponds to SLM output, while the rough spectral state corresponds to MLM output, as illustrated from the FPI output plots in Figure 3. When the cavity length was set so as to produce

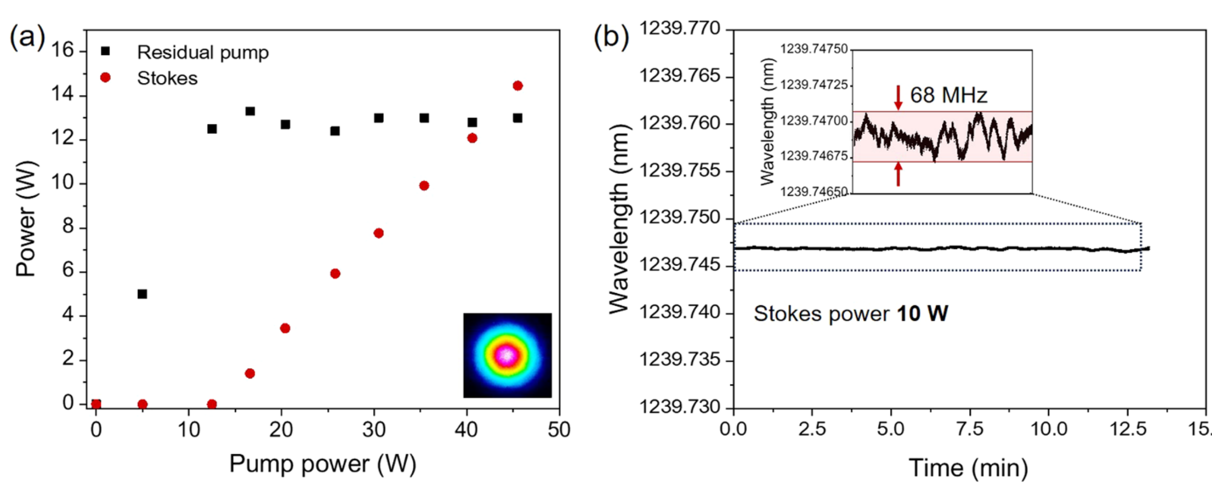

Figure 2. Plots showing (a) variation of the first Stokes field and residual fundamental powers with respect to incident fundamental (pump) power and (b) wavelength stability of the first Stokes field at an output power of 10 W and monitored over a period of 10 minutes.

https://doi.org/10.1017/hpl.2024.68 Published online by Cambridge University Press

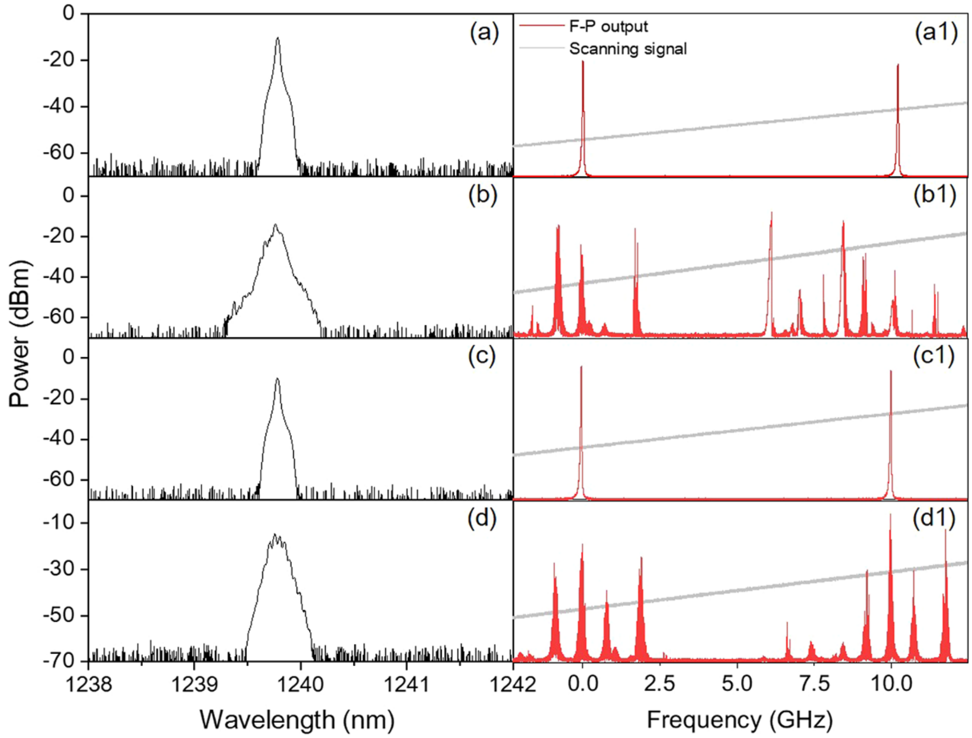

Figure 3. First Stokes output spectrum and longitudinal-mode structure for different Raman cavity lengths obtained by controlling the voltage applied to the PZT. Black represents the output spectrum and red represents the corresponding FPI transmission signal. From (a) to (c), the cavity length decreases incrementally by 690 nm.

SLM output, the fluctuation in the center frequency was of the order of tens of MHz, as shown in Figure 2(b).

Changes to the cavity length effectively scan the longitudinal modes of the cavity through the SRS gain profile, thus providing a means by which a single mode can have maximum gain, or two modes can have equal gain. Ultimately, this results in a transition between SLM and MLM Raman output as the cavity length is varied. Figure 4 outlines the relationship between the longitudinal modes of the cavity and the Raman gain at different cavity lengths. Let us focus on the condition whereby a longitudinal mode of the cavity is located at the center of the Raman gain spectrum, as illustrated in Figure 4(a). In the absence of SHB (as is the case in SRS) and with the fact that the linewidth of the pump/fundamental field is much narrower than the SRS gain bandwidth of diamond, depletion of the fundamental field takes place at the center of the SRS gain spectrum, and adjacent longitudinal modes reach gain saturation, thus preventing them from extracting energy from the fundamental field. This results in SLM Stokes output. When the cavity length is varied, the modes are swept through the Raman gain profile for the fixed fundamental wavelength. Also highlighted in Figure 4 is the condition where the longitudinal modes of the cavity are located at either side of the gain peak (Figure 4(b)). In this case, the two longitudinal modes closest to the gain center experience almost identical SRS gain, leading to approximately equal gain between the modes, in which case small system perturbations lead to multimode behavior.

For a cavity length that positions a longitudinal mode at the center of the SRS gain, SLM output can be achieved and this is represented by the state shown in Figure 4(c). Based on the results in Figure 3 and the schematic shown in Figure 4, it can be concluded that the first Stokes output can be made to vary between the SLM and MLM in a periodic fashion by changing the length of the cavity. We determined that this variation occurs with a period of approximately 690 nm (corresponding to a PZT voltage of ~2.6 V). The experimental result is slightly larger than the theoretical values ($\lambda/2 \approx 620$ nm, which corresponds to a free spectral range (FSR)). We posit that this may be due to thermal effects inside the cavity causing an increase in the cavity length of the experimental system[12]. Therefore, in the experiments, for each investigated power level, the length of the cavity was fine-tuned in order to produce SLM output at the first Stokes wavelength.

We used the delayed self-heterodyne interferometric (DSHI) method to determine the linewidth of the Raman output at maximum pump power. Using this method, the linewidth of the laser under test was determined by comparing the contrast difference between the first trough and the second peak (CDFTSP) of the coherence envelope[29,30]. Firstly, we measured the linewidth of the pump/fundamental laser using the DSHI method, employing

https://doi.org/10.1017/hpl.2024.68 Published online by Cambridge University Press

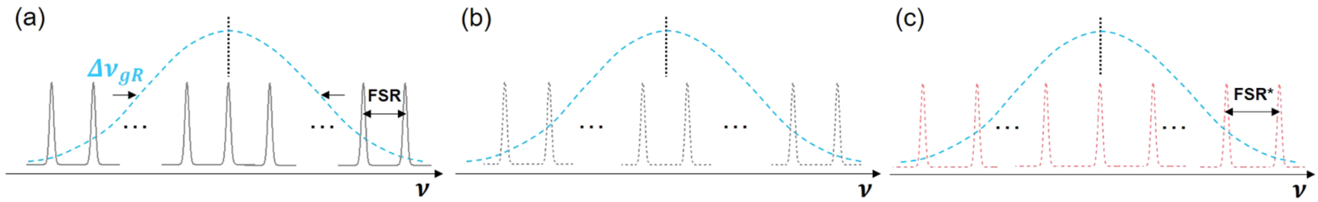

Figure 4. Schematic diagram showing the change in longitudinal-mode structure of the cavity in relation to the SRS gain for different cavity lengths. Gray and red represent the resonant cavity's intrinsic longitudinal modes, while blue represents the diamond Raman gain spectrum. To facilitate clearer comparison, the FSR has been appropriately magnified. (The Raman linewidth of diamond is ~40 GHz and the resonant cavity FSR is ~1.33 GHz. As a result, there are about 30 longitudinal modes within the Raman gain bandwidth.)

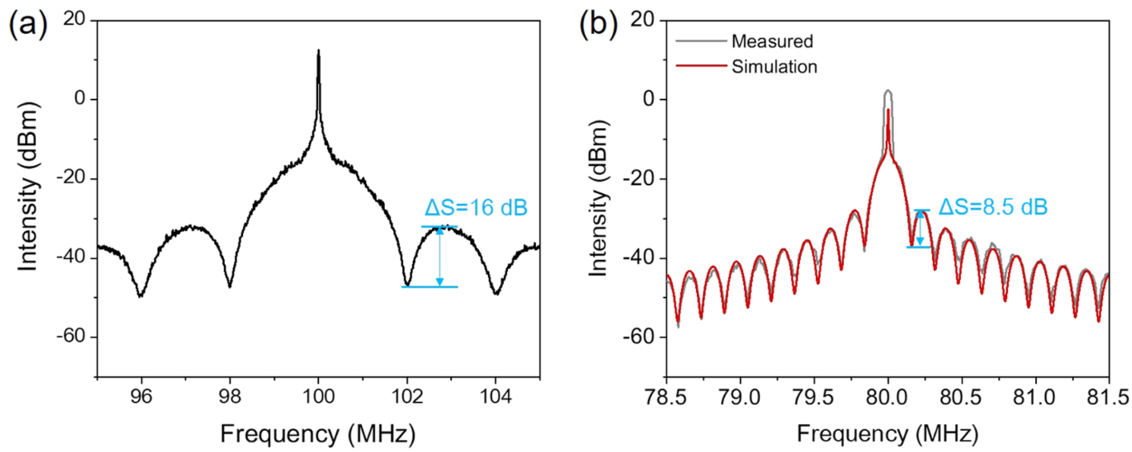

Figure 5. Plots showing (a) the coherence envelope function of the fundamental field and (b) a collection of coherence envelope functions of the first Stokes field at maximum pump power.

a 100 m delay fiber (Hi1060 Nufern) and an acousto-optic modulator (AOM) with a frequency shift of 100 MHz. The resulting coherence envelope is shown in Figure 5(a), where the CDFTSP is 16 dB. Through calculations, the linewidth was determined to be approximately 6.9 kHz. When the output Stokes field was SLM (achieved by adjusting the cavity length), the linewidth of the first Stokes field at maximum pump power was measured using a 1.3 km delay fiber and an AOM with a frequency shift of 80 MHz. The resulting coherence envelopes are presented in Figure 5(b). Here, the CDFTSP is 8.5 dB and remains almost identical across the different investigated output powers, indicating that the Raman linewidth did not vary with the output power. The corresponding first Stokes output linewidth was approximately 3.0 kHz, representing a narrowing by a factor of 2.3 in comparison to the linewidth of the fundamental field.

A range of delay fiber lengths were used in the linewidth measurements of the fundamental and Stokes fields. A shorter fiber length resulted in stronger coherence of the beat signal in the DSHI setup, leading to a more distinct coherence envelope. Fiber length needed to be selected based on the anticipated linewidth of the beam under examination. Too long a fiber could introduce flicker noise, while too short a fiber could cause excessive envelope size, affecting peak point accuracy. When a 100 m delay was used to examine the Stokes fields, the trough points were obscured by noise, resulting in overestimated linewidths. Therefore, for Stokes fields with narrower linewidths, we used a 1.3 km fiber for measurement.

2.2. *Generation of second Stokes emission*

The large Raman frequency shift of diamond can enable the generation of eye-safe 1.5 μm emission via cascaded Stokes shifting using a fundamental wavelength at approximately 1 μm[24,31,32]. In this work, we also investigated the generation of second Stokes emission at 1.5 μm, with a mind to produce a system optimized for narrow linewidth emission. To this effect, we modified our experimental setup by changing the IC to one that had a high-transmission coating for 1064 nm and a high-reflection coating for 1240 and 1485 nm. The OC was also changed so as to have a high-reflection coating for 1064 and 1240 nm, as well as a partially transmitting ($T = 45\%$) coating for 1485 nm. The IC and OCs had ROCs of 100 and 50 mm, respectively. The focal length of L3 was 100 mm, and the length of the cavity was approximately 153 mm. The corresponding fundamental, first Stokes and second Stokes beam waist radii in the diamond were 35, 48 and 53 μm, respectively.

Figure 6(a) shows the power-transfer characteristics of the first and second Stokes fields as a function of incident pump/fundamental power. At the maximum fundamental

https://doi.org/10.1017/hpl.2024.68 Published online by Cambridge University Press

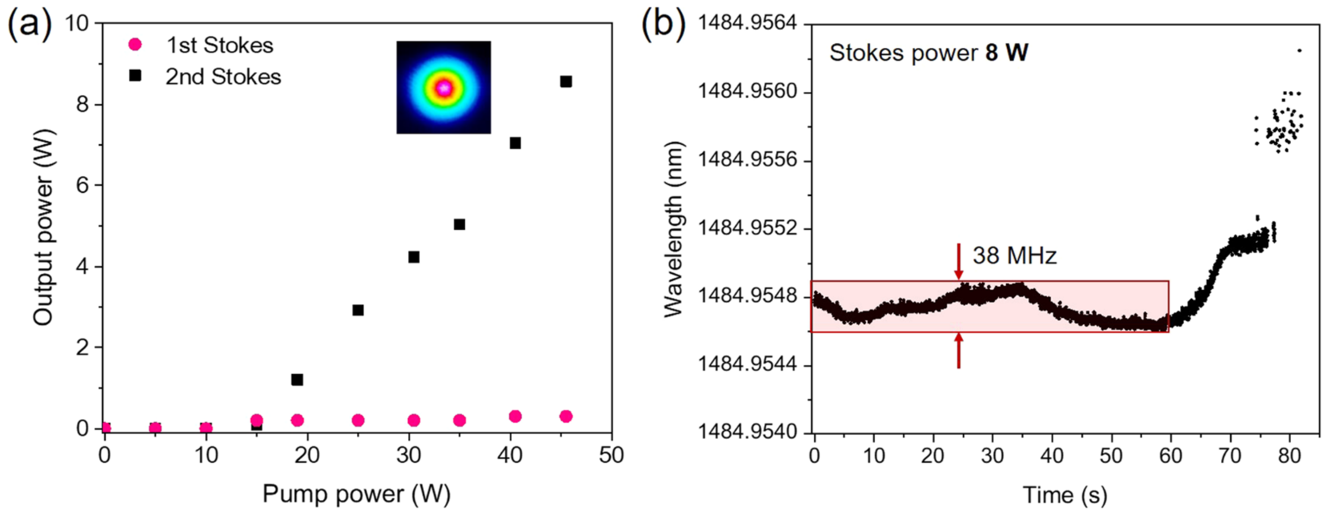

Figure 6. Plots showing (a) the power-transfer characteristics of the first and second Stokes outputs as a function of pump/fundamental power and (b) the wavelength stability of the second Stokes output at a power of 8 W.

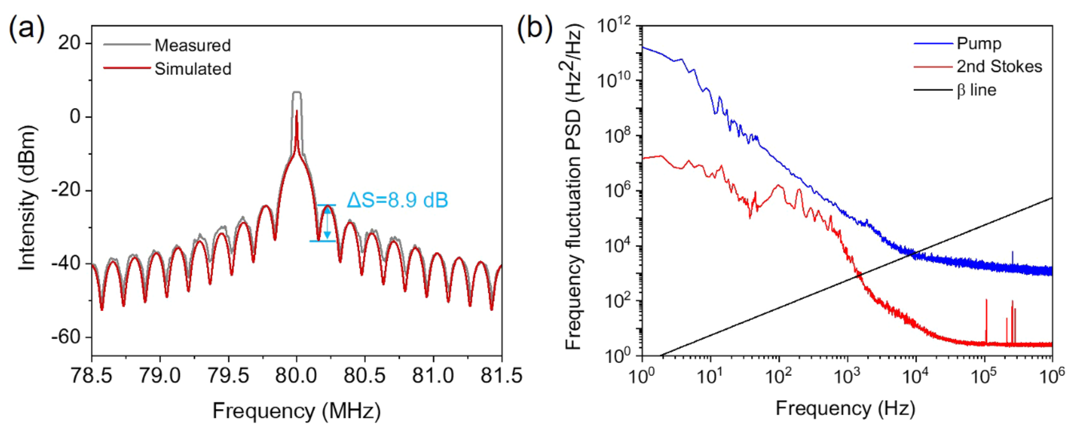

Figure 7. Plots showing (a) the coherence envelope functions of the second Stokes output at maximum pump power and (b) the noise characteristics of the fundamental and second Stokes outputs.

power of 45.5 W, a second Stokes output of 8.5 W was measured, corresponding to a conversion efficiency of 18.7%. The inset shows the spatial profile of the output second Stokes field at 1485 nm. Similar to observations made when optimizing for the first Stokes field, the cavity length also affected the longitudinal-mode output characteristics of the second Stokes field. Figure 6(b) shows the wavelength stability of the second Stokes field when it was emitted as an SLM and the output power was 8 W. It can be observed that the output wavelength fluctuated within a bandwidth of approximately 38 MHz over a 60-second period. Over longer time scales, due to temperature and environmental fluctuations, the output was found to fluctuate more significantly, leading to MLM output, as shown in Figure 3(b). This result highlights that the wavelength stability of the second Stokes field is lower than that of the first Stokes field in the first Stokes optimized system. We believe that this increased level of fluctuation is a result of additional thermal effects resulting from the Raman cascade process and the complex interactions that occur among the fundamental, first Stokes and second Stokes fields during this process.

Similar to the results presented for the first Stokes optimized system, we also used the DSHI method to measure the linewidth of the second Stokes output at different output power levels. Here, a 1.3 km delay fiber (SM28E Corning) was used; the coherence envelope functions of the second Stokes field at maximum pump power are shown in Figure 7(a). The results are similar to those achieved from the first Stokes optimized system and the CDFTSP values are nearly the same across the investigated power levels. The corresponding CDFTSP value was 8.9 dB, which corresponds to a linewidth of approximately 2.7 kHz. Compared to the first Stokes field, the linewidth of the second Stokes field shows a slight narrowing effect.

We utilized a commercial laser noise analyzer (SY1550-LDPD-C-T) to measure the noise of both the fundamental and second Stokes fields[33], which operates within two specific wavelength bands, 1 and 1.5 μm, as illustrated in Figure 7(b). It can be observed that across the entire measured frequency range, there is a significant improvement in the frequency noise performance of the second Stokes field because of the linewidth narrowing compared to the fundamental field. After the β line, there is a continued and significant reduction in the Stokes frequency noise; the white noise floor of second Stokes is suppressed by approximately 30 dB compared with that of the pump and it is approaching approximately 2.5 Hz^2/Hz corresponding to a fundamental linewidth of approximately 3.6 Hz[34]. The higher noise region observed in the range from 10^2 to 10^3 Hz is attributed to acoustic noise from the experimental environment. To the best of our knowledge, this represents the first time that linewidth measurements and noise analyses have been performed on a cascaded diamond Raman laser.

3. Conclusion

In conclusion, we have designed and characterized a narrow linewidth diamond Raman laser cavity pumped using a 1 μm laser to generate high-power, narrow linewidth emission at 1240 and 1485 nm. Through precise adjustment of the cavity length, we achieved matching of the cavity modes with the SRS gain of diamond to produce 1240 and 1485 nm outputs with linewidths of 3.0 and 2.7 kHz and corresponding maximum output powers of 14 and 8 W, respectively, and the linewidths are compressed by more than two times compared to the pump. The cascaded Raman output exhibited lower-frequency noise than the fundamental field across the entire measurement frequency range, the white noise floor of the second Stokes field is decreased by approximately three orders of magnitude compared to that of the pump and the corresponding fundamental linewidth reaches the level of hertz. In addition, the excellent thermal properties of diamond allowed the output performance to remain stable across a range of water-cooled temperatures (20°C ± 5°C). Although the commercial noise analyzer effectively demonstrated the noise spectrum, we believe further optimization is possible. In future work, we plan to implement the correlated self-heterodyne method[35] to enable precise ultra-low-noise detection. This study demonstrates the potential of diamond Raman lasers for producing high-power, narrow linewidth outputs at specific wavelengths, without the need for additional frequency-selective elements. We anticipate that such systems will play a crucial role in advancing the development of narrow linewidth lasers and related applications.

Acknowledgements

This work was supported by the National Natural Science Foundation of China (Nos. 62375076 and 61927815), the Natural Science Foundation of Tianjin City (No. 22JCYBJC01100), the Natural Science Foundation of Hebei Province (No. F2023202063), the Shijiazhuang Overseas Talents Introduction Project (No. 20230004) and the Funds for Basic Scientific Research of Hebei University of Technology (No. JBKYTD2201). The authors acknowledge Professor Richard Mildren (Macquarie University) and Dr. Fei Yang (Shanghai Institute of Optics and Fine Mechanics, Chinese Academy of Sciences) for valuable comments and helpful discussions.

References

1. B. P. Abbott, R. Abbott, T. D. Abbott, M. R. Abernathy, F. Acernese, K. Ackley, C. Adams, T. Adams, P. Addesso,R. X. Adhikari, V. B. Adya, C. Affeldt, M. Agathos, K. Agatsuma, N. Aggarwal, O. D. Aguiar, L. Aiello, A. Ain, P. Ajith, B. Allen, A. Allocca, P. A. Altin, S. B. Anderson, W. G. Anderson, K. Arai, M. A. Arain, M. C. Araya, C. C. Arceneaux, J. S. Areeda, N. Arnaud, K. G. Arun, S. Ascenzi, G. Ashton, M. Ast, S. M. Aston, P. Astone, P. Aufmuth, C. Aulbert, S. Babak, P. Bacon, M. K. M. Bader, P. T. Baker, F. Baldaccini, G. Ballardin, S. W. Ballmer, J. C. Barayoga, S. E. Barclay, B. C. Barish, D. Barker, F. Barone, B. Barr, L. Barsotti, M. Barsuglia, D. Barta, J. Bartlett, M. A. Barton, I. Bartos, R. Bassiri, A. Basti, J. C. Batch, C. Baune, V. Bavigadda, M. Bazzan, B. Behnke, M. Bejger, C. Belczynski, A. S. Bell, C. J. Bell, B. K. Berger, J. Bergman, G. Bergmann, C. P. L. Berry, D. Bersanetti, A. Bertolini, J. Betzwieser, S. Bhagwat, R. Bhandare, I. A. Bilenko, G. Billingsley, J. Birch, R. Birney, O. Birnholtz, S. Biscans, A. Bisht, M. Bitossi, C. Biwer, M. A. Bizouard, J. K. Blackburn, C. D. Blair, D. G. Blair, R. M. Blair, S. Bloemen, O. Bock, T. P. Bodiya, M. Boer, G. Bogaert, C. Bogan, A. Bohe, P. Bojtos, C. Bond, F. Bondu, R. Bonnand, B. A. Boom, R. Bork, V. Boschi, S. Bose, Y. Bouffanais, A. Bozzi, C. Bradaschia, P. R. Brady, V. B. Braginsky, M. Branchesi, J. E. Brau, T. Briant, A. Brillet, M. Brinkmann, V. Brisson, P. Brockill, A. F. Brooks, D. A. Brown, D. D. Brown, N. M. Brown, C. C. Buchanan, A. Buikema, T. Bulik, H. J. Bulten, A. Buonanno, D. Buskulic, C. Buy, R. L. Byer, M. Cabero, L. Cadonati, G. Cagnoli, C. Cahillane, J. C. Bustillo, T. Callister, E. Calloni, J. B. Camp, K. C. Cannon, J. Cao, C. D. Capano, E. Capocasa, F. Carbognani, S. Caride, J. C. Diaz, C. Casentini, S. Caudill, M. Cavaglià, F. Cavalier, R. Cavalieri, G. Cella, C. B. Cepeda, L. C. Baiardi, G. Cerretani, E. Cesarini, R. Chakraborty, T. Chalermsongsak, S. J. Chamberlin, M. Chan, S. Chao, P. Charlton, E. Chassande-Mottin, H. Y. Chen, Y. Chen, C. Cheng, A. Chincarini, A. Chiummo, H. S. Cho, M. Cho, J. H. Chow, N. Christensen, Q. Chu, S. Chua, S. Chung, G. Ciani, F. Clara, J. A. Clark, F. Cleva, E. Coccia, P. F. Cohadon, A. Colla, C. G. Collette, L. Cominsky, M. Constancio, A. Conte, L. Conti, D. Cook, T. R. Corbitt, N. Cornish, A. Corsi, S. Cortese, C. A. Costa, M. W. Coughlin, S. B. Coughlin, J. P. Coulon, S. T. Countryman, P. Couvares, E. E. Cowan, D. M. Coward, M. J. Cowart, D. C. Coyne, R. Coyne, K. Craig, J. D. E. Creighton, T. D. Creighton, J. Cripe, S. G. Crowder, A. M. Cruise, A. Cumming, L. Cunningham, E. Cuoco, T. D. Canton, S. L. Danilishin, S. D Antonio, K. Danzmann, N. S. Darman, C. F. Da Silva Costa, V. Dattilo, I. Dave, H. P. Daveloza, M. Davier, G. S. Davies, E. J. Daw, R. Day, S. De, D. DeBra, G. Debreczeni, J. Degallaix, M. De Laurentis, S. Deléglise, W. Del Pozzo, T. Denker, T. Dent, H. Dereli, V. Dergachev, R. T. DeRosa, R. De Rosa, R. DeSalvo, S. Dhurandhar, M. C. Díaz, L. Di Fiore, M. Di Giovanni, A. Di Lieto, S. Di Pace, I. Di Palma, A. Di Virgilio, G. Dojcinoski, V.

Dolique, F. Donovan, K. L. Dooley, S. Doravari, R. Douglas, T. P. Downes, M. Drago, R. W. P. Drever, J. C. Driggers, Z. Du, M. Ducrot, S. E. Dwyer, T. B. Edo, M. C. Edwards, A. Effler, H. B. Eggenstein, P. Ehrens, J. Eichholz, S. S. Eikenberry, W. Engels, R. C. Essick, T. Etzel, M. Evans, T. M. Evans, R. Everett, M. Factourovich, V. Fafone, H. Fair, S. Fairhurst, X. Fan, Q. Fang, S. Farinon, B. Farr, W. M. Farr, M. Favata, M. Fays, H. Fehrmann, M. M. Fejer, D. Feldbaum, I. Ferrante, E. C. Ferreira, F. Ferrini, F. Fidecaro, L. S. Finn, I. Fiori, D. Fiorucci, R. P. Fisher, R. Flaminio, M. Fletcher, H. Fong, J. D. Fournier, S. Franco, S. Frasca, F. Frasconi, M. Frede, Z. Frei, A. Freise, R. Frey, V. Frey, T. T. Fricke, P. Fritschel, V. V. Frolov, P. Fulda, M. Fyffe, H. A. G. Gabbard, J. R. Gair, L. Gammaitoni, S. G. Gaonkar, F. Garufi, A. Gatto, G. Gaur, N. Gehrels, G. Gemme, B. Gendre, E. Genin, A. Gennai, J. George, L. Gergely, V. Germain, A. Ghosh, A. Ghosh, S. Ghosh, J. A. Giaime, K. D. Giardina, A. Giazotto, K. Gill, A. Glaefke, J. R. Gleason, E. Goetz, R. Goetz, L. Gondan, G. González, J. M. G. Castro, A. Gopakumar, N. A. Gordon, M. L. Gorodetsky, S. E. Gossan, M. Gosselin, R. Gouaty, C. Graef, P. B. Graff, M. Granata, A. Grant, S. Gras, C. Gray, G. Greco, A. C. Green, R. J. S. Greenhalgh, P. Groot, H. Grote, S. Grunewald, G. M. Guidi, X. Guo, A. Gupta, M. K. Gupta, K. E. Gushwa, E. K. Gustafson, R. Gustafson, J. J. Hacker, B. R. Hall, E. D. Hall, G. Hammond, M. Haney, M. M. Hanke, J. Hanks, C. Hanna, M. D. Hannam, J. Hanson, T. Hardwick, J. Harms, G. M. Harry, I. W. Harry, M. J. Hart, M. T. Hartman, C. J. Haster, K. Haughian, J. Healy, J. Heefner, A. Heidmann, M. C. Heintze, G. Heinzel, H. Heitmann, P. Hello, G. Hemming, M. Hendry, I. S. Heng, J. Hennig, A. W. Heptonstall, M. Heurs, S. Hild, D. Hoak, K. A. Hodge, D. Hofman, S. E. Hollitt, K. Holt, D. E. Holz, P. Hopkins, D. J. Hosken, J. Hough, E. A. Houston, E. J. Howell, Y. M. Hu, S. Huang, E. A. Huerta, D. Huet, B. Hughey, S. Husa, S. H. Huttner, T. Huynh-Dinh, A. Idrisy, N. Indik, D. R. Ingram, R. Inta, H. N. Isa, J. M. Isac, M. Isi, G. Islas, T. Isogai, B. R. Iyer, K. Izumi, M. B. Jacobson, T. Jacqmin, H. Jang, K. Jani, P. Jaranowski, S. Jawahar, F. Jiménez-Forteza, W. W. Johnson, N. K. Johnson-McDaniel, D. I. Jones, R. Jones, R. J. G. Jonker, L. Ju, K. Haris, C. V. Kalaghatgi, V. Kalogera, S. Kandhasamy, G. Kang, J. B. Kanner, S. Karki, M. Kasprzack, E. Katsavounidis, W. Katzman, S. Kaufer, T. Kaur, K. Kawabe, F. Kawazoe, F. Kéfélian, M. S. Kehl, D. Keitel, D. B. Kelley, W. Kells, R. Kennedy, D. G. Keppel, J. S. Key, A. Khalaidovski, F. Y. Khalili, I. Khan, S. Khan, Z. Khan, E. A. Khazanov, N. Kijbunchoo, C. Kim, and J. Zweizig (LIGO Scientific Collaboration and Virgo Collaboration), Phys. Rev. Lett. **116**, 061102 (2016).
2. X. Su, C. Tian, X. Deng, Q. Li, C. Xie, and K. Peng, Phys. Rev. Lett. **117**, 240503 (2016).
3. D. B. Calia, Y. Feng, W. Hackenberg, R. Holzlöhner, L. Taylor, and S. Lewis, Messenger **139**, 12 (2010).
4. T. W. Hänsch and A. L. Schawlow, Opt. Commun. **13**, 68 (1975).
5. C. Tang, H. Statz, and G. de Mars, J. Appl. Phys. **34**, 2289 (1963).
6. T. J. Kane and R. L. Byer, Opt. Lett. **10**, 65 (1985).
7. J. J. Zayhowski and A. Mooradian. Opt. Lett. **14**, 24 (1989).
8. S. A. Collins and G. R. White, Appl. Opt. **2**, 448 (1963).
9. J. E. Bjorkholm and H. G. Danielmeyer, Appl. Phys. Lett. **15**, 171 (1969).
10. H. Rong, R. Jones, A. Liu, O. Cohen, D. Hak, A. Fang, and M. Paniccia, Nature **433**, 725 (2005).
11. C. Y. Lee, C. Chang, P. Tuan, C. Y. Cho, K. Huang, and Y. Chen, Opt. Lett. **40**, 1996 (2015).
12. O. Lux, S. Sarang, O. Kitzler, D. J. Spence, and R. P. Mildren, Optica **3**, 876 (2016).
13. Y. Liu, C. Zhu, Y. Sun, R. P. Mildren, Z. Bai, B. Zhang, W. Chen, D. Chen, M. Li, X. Yang, and Y. Feng, High Power Laser Sci. Eng. **11**, e72 (2023).
14. D. Jin, Z. Bai, Z. Lu, R. Fan, Z. Zhao, X. Yang, Y. Wang, and R. P. Mildren, Opt. Lett. **47**, 5360 (2022).
15. D. Jin, Z. Bai, Z. Zhao, Y. Chen, W. Fan, Y. Wang, R. P. Mildren, and Z. Lu, High Power Laser Sci. Eng. **11**, e47 (2023).
16. I. Friel, S. L. Geoghegan, D. J. Twitchen, and G. A. Scarsbrook, Proc. SPIE **7838**, 783819 (2010).
17. R. S. Balmer, J. R. Brandon, S. L. Clewes, H. K. Dhillon, M. Dodson, I. Friel, P. N. Inglis, T. D. Madgwick, M. L. Markham, T. P. Mollart, N. Perkins, G. A. Scarsbrook, D. J. Twitchen, A. J. Whitehead, J. J. Wilman, and S. M. Woollard, J. Phys. Condens. Matter. **21**, 364221 (2009).
18. Z. Bai, R. J. Williams, H. Jasbeer, S. Sarang, O. Kiteler, A. Mckay, and R. P. Mildren, Opt. Lett. **43**, 563 (2018).
19. H. Chen, Z. Bai, Y. Cai, X. Yang, J. Ding, Y. Qi, B. Yan, Y. Li, Y. Wang, Z. Lu, and R. P. Mildren, Appl. Phys. Lett. **122**, 092202 (2023).
20. F. Lu, Funct. Diamond **2**, 119 (2022).
21. S. Sarang, O. Kitzler, O. Lux, Z. Bai, R. J. Williams, D. J. Spence, and R. P. Mildren, OSA Continuum **2**, 1028 (2019).
22. Y. Sun, M. Li, O. Kitzler, R. P. Mildren, Z. Bai, H. Zhang, J. Lu, Y. Feng, and X. Yang, Laser Phys. Lett. **19**, 125001 (2022).
23. Z. Bai, R. J. Williams, O. Kitzler, S. Sarang, D. J. Spence, and R. P. Mildren, Opt. Express **26**, 19797 (2018).
24. O. Lux, S. Sarang, R. J. Williams, A. Mckay, and R. P. Mildren, Opt. Express **24**, 27812 (2016).
25. X. Yang, O. Kitzler, D. J. Spence, R. J. Williams, Z. Bai, S. Sarang, L. Zhang, Y. Feng, and R. P. Mildren, Opt. Lett. **44**, 839 (2019).
26. X. Yang, Z. Bai, D. Chen, W. Chen, Y. Feng, and R. P. Mildren, Opt. Express **29**, 29449 (2021).
27. A. Sabella, J. A. Piper, and R. P. Mildren, Opt. Lett. **35**, 3874 (2010).
28. Z. Bai, Z. Zhang, K. Wang, J. Gao, Z. Zhang, X. Yang, Y. Wang, Z. Lu, and R. P. Mildren, Nanomaterials **11**, 1572 (2021).
29. Z. Zhao, Z. Bai, D. Jin, Y. Qi, J. Ding, B. Yan, Y. Wang, Z. Lu, and R. P. Mildren, Opt. Express. **30**, 30600 (2022).
30. Z. Zhao, Z. Bai, D. Jin, X. Chen, Y. Qi, J. Ding, B. Yan, Y. Wang, Z. Lu, and R. P. Mildren, Micromachines **13**, 1311 (2022).
31. H. Chen, Y. Cui, X. Li, B. Zhang, Y. Cai, J. Ding, Y. Qi, B. Yan, Y. Wang, Z. Lu, and Z. Bai, Funct. Diamond **3**, 2282527 (2023).
32. Y. Li, Z. Bai, H. Chen, D. Jin, X. Yang, Y. Qi, J. Ding, Y. Wang, and Z. Lu, Results Phys. **16**, 102853 (2020).
33. D. Xu, F Yang, D. Chen, F Wei, H. Cai, Z. Fang, and R. Qu, Opt. Express **23**, 22386 (2015).
34. S. Gundavarapu, G. M. Brodnik, M. Puckett, T. Huffman, D. Bose, R. Behunin, J. Wu, T. Qiu, C. Pinho, N. Chauhan, J. Nohava, P. T. Rakich, K. D. Nelson, M. Salit, and D. J. Blumenthal, Nat. Photonics **13**, 60 (2019).
35. Z. Yuan, H. Wang, P. Liu, B. Li, B. Shen, M. Gao, L. Chang, W. Jin, A. Feshali, M. Paniccia, J. Bowers, and K. Vahala, Opt. Express, **30**, 25147 (2022).

https://doi.org/10.1017/hpl.2024.68 Published online by Cambridge University Press